Research Square

Preprints are preliminary reports that have not undergone peer review.
They should not be considered conclusive, used to inform clinical practice,
or referenced by the media as validated information.

PAM_16A activates the TMEM16A chloride channel by increasing its calcium affinity

Tanadet Pipatpolkai

tanadet.pipatpolkai@ntu.edu.sg

Nanyang Technological University https://orcid.org/0000-0001-5396-4784

Article

Keywords:

Posted Date: August 27th, 2026

DOI: https://doi.org/10.21203/rs.3.rs-10481839/v1

License: This work is licensed under a Creative Commons Attribution 4.0 International License.
Read Full License

Additional Declarations: There is **NO** Competing Interest.

Main Manuscript for

PAM_16A activates the TMEM16A chloride channel by increasing its calcium affinity

This PDF file includes:

Main Text

Figures 1 to 4

Abstract

TMEM16A is a calcium-activated chloride channel, making it a promising therapeutic target for diseases characterised by impaired chloride influx, such as cystic fibrosis. While novel allosteric activators such as PAM_16A have been developed, their binding sites and mechanisms of action remain unknown. Here, I used a multi-tiered computational approach: Generative AI (Chai-1), MARTINI-3 coarse-grained molecular dynamics (MD), docking and all-atom MD were used to identify the PAM_16A binding site. Free energy perturbation (FEP) and Fluctuation Amplification of Specific Traits (FAST) adaptive sampling were used to calculate the effect of PAM_16A on calcium affinity and efficacy. Here, I show that PAM_16A binds stably in the intracellular region near the calcium-binding site. FEP calculations reveal that PAM_16A increases TMEM16A's affinity for calcium by approximately 10-14 kJ/mol through dehydration of the binding pocket. Furthermore, FAST adaptive sampling shows that PAM_16A slightly favours the opening of the steric gate. Thus, this work disentangles affinity from efficacy, demonstrating that PAM_16A activates TMEM16A by increasing its calcium affinity. Thus, this study provides a robust computational framework combining adaptive sampling and FEP to predict the pharmacological properties of ion channel modulators prior to experimental mutagenesis.

Introduction

TMEM16A (or Anoctamin-1) is a calcium-activated chloride channel, and is responsible for chloride influx in the smooth muscle and epithelial cell [1]. In diseases where the influx of chloride ions is impaired, such as cystic fibrosis, targeting the activatory mechanism of TMEM16A provides a potential therapeutic opportunity for the disease [2].

TMEM16A is activated by Ca^{2+} [3-5] and the opening of the outer gate is modulated by phosphatidylinositol-4,5-bisphosphate (PIP_2) [6-8]. The Ca^{2+} binding site is located at the bottom half of the TM6, whereas the PIP_2 binding site is located at the interface between TM4-5. The binding of Ca^{2+} introduce a further kink in TM6 and the opening at the lower half of the channel, known as the steric gate [9-11]. Ca^{2+} also attracts chloride and lower energy barrier for chloride permeation, as known as the electrostatic gate [12]. Both Ca^{2+} and PIP_2 binding has been shown to open the the outer pore, allowing TMEM16A-specific drug, such as anthracene-9-carboxylate (A9C), to enter its binding site [13].

Over the last two decades, the structures of TMEM16x family protein have been determined. Those include the dual scramblase and chloride channel *Nectria haematococca* TMEM16 (nhTMEM16); the TMEM16A in both apo and calcium-bound non-conductive conformation [14,15], gain-of-function mutation (I551A) [16], or the open state with pore blocker 1-hydroxy-3-(trifluoromethyl)pyrido[1,2-a]benzimidazole-4-carbonitrile (1PBC) [17]. In addition to the TMEM16F, lipid scramblase has been solved in the apo state and in complex with niclosamide [18]. Until now, there is no structure of TMEM16A with bound synthetic activators and thus, a mission to identify the binding site and the activatory mechanism of synthetic ligands using artificial intelligence (AI) and molecular dynamics (MD) simulation has become an attractive approach to the problem.

The recent explosion of virtual screening tools has opened up multiple opportunities for high-affinity generative drug design. Most tools focus primarily on the affinity of the drugs, and is lacking on providing the drug efficacy for TMEM16A activation. In this study, I identified the PAM_16A binding site using both a generative AI method and coarse-grained molecular dynamics simulation. The experimental data suggested that PAM_16A increases TMEM16A sensitivity to Ca^{2+}, whilst maintaining the constant channel unitary

conductance. The binding site of TMEM16A was identified using coarse-grained MD (CG) simulation, traditional flexible docking, and AI-generated binding poses using Chai-1, and the stability was further validated using extensive all-atom MD simulation. Furthermore, Free energy perturbation (FEP) was used to assess the effect of PAM_16A on TMEM16A affinity to calcium, and using Fluctuation Amplification of Specific Traits (FAST) adaptive sampling to calculate the effect of PAM_16A on the kinetics of channel opening, and the thermodynamic stability of channel opening. Overall, this work highlights the power of molecular dynamics simulation to provide the mechanistic insight to distinguish between affinity and efficacy, for chemical screening and filling in the missing information, which might be far out of reach by AI at the current stage of technology.

Results

PAM_16A binds next to the calcium-binding site

The first goal of this study is to determine the binding site of the PAM_16A activator compound. The clue from the previous study, a slightly long perfusion time (15 s) hinted that the molecule may bind intracellularly. In this study, I used three different approaches to gain insight into the PAM_16A binding site: an AI-based method (Chai1), MARTINI-3 coarse-grained MD simulations and docking followed by 15 repeats of 300 ns all-atom MD simulations to gain insight into the putative binding site prior to any further computational validation.

Using Chai-1, 1 TMEM16A monomer is chosen as the target for a 20 PAM_16A compound. Given that TMEM16A is an obligate dimer, I note that using a monomer for the binding site may not capture the site at the binding interface. From the monomer, the binding site for PAM_16A is clustered between 2 intracellular locations. (1) At the chloride permeation pathway at the steric gate, between TM4 and TM6. (2) In front of the calcium-binding site on the TM6 (Figure 1A). The scores on both sites are similar, raising questions about the validity and reliability of the prediction (Supplementary Table 1). I then used a physics-based approach to identify the PAM_16A binding site. Using AutoMartini3, I generated a CG force field for PAM_16A (Supplementary Table 2, Supplementary Figure 1), randomly placed 20 PAM_16A molecules in the simulation box, and simulated for 10 μs across 10 replicates (Figure 1B). The density of the coarse-grained ligand was then calculated using VolMap. Here, the density map is also primarily clustered at the calcium-binding site and the steric gate, consistent with the Chai-1 prediction. I hypothesised that the drug could not block the pore; otherwise, the ion would not be able to permeate across the channel (Figure 1B). Thus, PAM_16A is likely accessing its binding site through the intracellular gate and binds near the calcium-binding site. Thus, a docking box is centred at the calcium-binding site with the docking space extended to the intracellular gate. Here, I show that the top-ranked docking pose is located at the calcium-binding site, thus supporting this hypothesis (Figure 1D, 1E).

To test whether PAM_16A can bind stably near the calcium-binding site, 300 ns simulations with 15 repeats were conducted to ensure that the docking pose is not trapped in local minima. Here, PAM_16A remains stable throughout the simulations, with most root-mean-square deviation (RMSD) values below 0.4 nm (Figure 1F). The drug binding pocket consists mainly of the hydrophobic residues, including F653, I551, L746 and I657. The chlorine atom is co-ordinated with K661. The hydrogen bond is formed between K671 and the phenol moiety, and K741, N650 and E654 form interactions with the amide groups (Figure 1G). The combination of pi-stacking and several hydrogen bonds led to the overall stability within the drug binding site. Interestingly, except for E654, no other residues share the residues known to coordinate with the calcium ion, just residues within the proximity. Together, I conclude that PAM_16A binds near the calcium-binding site at the bottom of the TM6 helix.

PAM_16A increases TMEM16A affinity to calcium

The next question is how PAM_16A activates the TMEM16A channel. The activation could be achieved by enhancing the intrinsic properties of the channel, such as unitary conductance and open probability, in the calcium-free state or the calcium-bound state. The drug could also increase TMEM16A affinity to calcium [19]. A recent experimental study suggested that PAM_16A increases the sensitivity of the channel to calcium activation [19]. The work also shows that the drug does not affect unitary conductance of the channel. Given the proximity to the calcium-binding site, I hypothesise that PAM_16A may increase calcium affinity to the site.

To quantify calcium affinity, I used free energy perturbation (FEP) to compute the absolute binding free energy of calcium, decoupling each ion to a non-interacting dummy particle both in the binding site and in bulk water (n = 3; λ spacing and sampling time were chosen to give good MBAR phase-space overlap between windows; Supplementary Figure 2-3). Each ion was held in its pocket with a flat-bottom restraint and perturbed independently, one at a time, and a Rocklin-type correction was applied to account for the finite box size. I first asked in what order the two ions occupy the site in the absence of the drug. Perturbing a single calcium ion placed alternately at the top or the bottom site gave very similar binding free energies (−149 ± 4 vs −152 ± 7 kJ/mol; Figure 2A), indicating equal

affinity when the partner site is empty; when the partner site was occupied, however, the top site became substantially weaker (−114 ± 5 kJ/mol), consistent with electrostatic repulsion between the two ions and a loss of coordination, as most acidic residues are already engaged by the bottom ion. The absolute values are non-physiological, reflecting the known overestimation of divalent-ion interactions in the CHARMM36m force field and, as expected, the ionic charge perturbation. In addition, the perturbation drift slowly and do not fully converge; the conclusions therefore rest on reproducibility across three independent replicates and on the relative ΔΔG, in which systematic sampling bias largely cancels (Supplementary Figure 3). Overall, these results indicate that the top site is occupied first, followed by the bottom site — a sequential, revolver-like loading of the two ions.

Our next goal is to calculate the effect of PAM_16A on calcium affinity. Here, the calcium affinity is calculated in the presence of PAM_16A at the binding site. The calcium affinity increases by approximately 10-14 kJ/mol (-149 ± 4 kJ/mol vs -159 ± 6 kJ/mol) (Figure 2B). This is likely because more channels in the macroscopic patch are bound to calcium, leading to an overall increase in current and thus explaining the mechanism of how PAM_16A activates TMEM16A.

I then investigate the molecular reasoning for the increase in calcium affinity to the site. Hence, the minimum distance between PAM_16A and the calcium ion from 15 repeats of 300 ns simulations was calculated. Here, the result shows that PAM_16A is 0.6 nm from the calcium ion, suggesting that the drug may mildly and directly increase the affinity of calcium ions. Given the hydrophobic nature of the drug molecule, it is also possible to postulate that the drug excludes water from the calcium-binding pocket, thereby increasing affinity by reducing the dielectric constant of the environment. Thus, I compared the local dynamics of the calcium-binding site and the hydration at 8 Å radius around the calcium ion. The simulation shows that the side-chain dynamics of the residues coordinating calcium are significantly reduced, particularly at D738, E705, and E734 (Figure 2D). Although the reduction in fluctuation is less than 1 Å, it remains consistent across 15 replicates. In addition, I count the number of molecules within 8 Å of calcium and show that the region becomes less hydrated upon PAM_16A binding (16 vs 12 water molecules) (Figure 2E). Thus, this explains the mechanism of the increased affinity by reducing the

side chain fluctuation, as the region becomes less hydrated and thus will directly affect the local dielectric constant. Together, I conclude that PAM_16A increases affinity for calcium at its respective binding site.

PAM_16A does not stabilise the opening of TMEM16A

Our next goal is to examine whether PAM_16A affects the opening probability or the channel kinetics of the TMEM16A channel independent of calcium. I set up two systems, both with calcium within the binding site, but with and without the drug. PIP_2 is not added to the system, as PIP_2 has previously shown to have no effect on PAM_16A action [19]. I then drive the channel towards the opening of the outer gate using fluctuation amplification of specific traits (FAST) adaptive sampling. In FAST adaptive sampling, a set of distances between TM4-6 is treated as a key feature to be maximised, thereby favouring the dilation of the outer pore (Figure 3A). The free energy landscape (FEL), describing the sampled conformations in each basin, was built and reweighted using Markov state modelling (MSM). The convergence was assessed, and process kinetics were calculated using a lag time of 10 ns; convergence was evaluated using the Chapman-Kolmogorov (CK) test (Supplementary Figure 4-5). The FEL was projected along the time-lagged Independent Component (tIC) based on the tIC Analysis (tICA) in the presence and the absence of PAM_16A. The distance between V543 and I640, the key residue at the outer gate, is a metric for assessing the channel's openness along the FEL. In both sets of simulations, three clear minima is observed, corresponding to 3 sets of outer gate distances (Figure 3B, 3C). The depth of the minima, both in the presence and the absence of PAM_16A, remains relatively similar in both conditions. This suggested that PAM_16A does not influence the open probability of the channel in the presence of calcium, in agreement of the experimental results.

Given the close proximity of PAM_16A to the calcium-binding site, the next goal is to investigate whether PAM_16A has an additional effect on the opening of the steric gate by introducing a further kink on the TM6 at G656 (Figure 3D). The kink at G656 has previously been shown to be associated with the opening of the channel's steric gate. Our simulation shows that, at the distance where the outer gate is open, the steric gate kink

angle is approximately 160 degrees, suggesting that the drug may stabilise the opening of the steric gate and increase affinity for calcium.

Next, I investigated the effect of PAM_16A on TMEM16A channel opening in the absence of calcium (Figure 4A). In all cases, the MSM does not quite converge, and FAST adaptive sampling is also not able to access the opening at the outer mouth of the pore (Supplementary Figure 6-7). This highlight the importance of calcium in the opening mechanism of TMEM16A, even in the presence of the drug molecule. Thus, I diverge my attention to see whether PAM_16A is able to open the outer mouth of the pore and/or stabilise the kinking angle of the steric gate with the help of adaptive sampling, which may explain the slight increase in the experimental open probability from 0.1 to 0.3. Here, I show that a kink angle of approximately 160-170 degrees is observed on TM6, even with the pore closed. Thus, it is possible that PAM_16A helps stabilise the steric gate in a similar fashion to calcium when calcium is absent, but with a much weaker effect. Also, calcium is crucially required for the dilation of the outer mouth of the pore. Taken together, this mechanistically explains that PAM_16A binds to TM6 and stabilises the steric gate. The binding of PAM_16A increases calcium affinity to the binding site and thus increases the activatory effect of TMEM16A by calcium.

Discussion

The PAM_16A is a direct allosteric activator of TMEM16A, which has been previously shown to be a potential treatment for cystic fibrosis. By activating TMEM16A, the channel can compensate for a defect in CFTR and thus, provide a potential treatment for the disease. Another application of PAM_16A is its therapeutic use for orthostatic hypotension. Another activator, such as E_{act}, has been previously shown to work on another ion channel, such as TRPV1. However, the binding site for PAM_16A is currently not known. In this study, I used both an AI and a physics-driven approach to identify the binding site for the PAM_16A on TMEM16A. Subsequently, free-energy perturbation and FAST adaptive sampling were used to validate the binding site and assess the effect of PAM_16A on the affinity and efficacy of calcium-activated TMEM16A.

Identification of ligand-binding sites on ion channels has been conducted using multiple approaches. Those include the traditional physics-based docking by Autodock VINA, flooding of ligand of interest in both coarse-grained and all-atom systems and recently, generative AI approaches such as Chai-1 and AlphaFold3 have also been commonly used to identify ligand binding sites. Different methods highlight differences in their reliability and, more importantly, the cost required to perform the calculation. Docking via a physics-based approach offers the fastest output of all physics-based methods, but has only recently been overtaken by AI. Combinations of both methods to validate against each other, with support from the experimental data. The more expensive approach is to develop a novel coarse-grained model for the ligand and conduct molecular dynamics simulations. The bottleneck, however, used to lie in the parameterisation of the coarse-grained ligand. That bottleneck has now been lifted by tools such as AutoMartini3 and a much-needed improvement in fine-tuning of the interaction of the coarse-grain forcefield in Martini3. The most expensive route is the flooding simulations with an all-atom ligand, which have previously been attempted on Piezo1 and have also successfully yielded a reliable binding site for Yoda1. In this study, I have combined three approaches: Chai-1 AI-based prediction and coarse-grained MD simulation to scope the PAM_16A binding site region. The site was then further refined through docking and extensive 15-repetitive MD simulations. Our binding site is located at the intracellular region, near the calcium

binding site – which is in agreement with the slower perfusion time in the electrophysiological set-up in the previous study.

Our goal is to understand the mechanism of PAM_16A activation, given that the drug increases the TMEM16A current influx. Thus, there are three intrinsic parameters: the unitary conductance, the number of channels on the patch and the open probability of the channel. The extrinsic parameters to be considered are the open probability of the channel after calcium binding (gating or efficacy) or the direct increase in calcium affinity. The experimental data highlight that PAM_16A increases TMEM16A calcium-dependent gating as the channel requires lower calcium concentrations to be activated. The study also used noise analysis to show that the drug does not affect the TMEM16A unitary conductance or the open probability at a saturated calcium concentration. Here, the simulation shows that the drug is not near the chloride permeation pathway but is located near the calcium-binding site.

To disentangle affinity from efficacy, I used FEP to calculate the effect of PAM_16A on the channel's calcium affinity. The absolute binding free energy of calcium is clearly overestimated by approximately 80 kJ/mol due to the parameterisation of the CHARMM36m force field and the artefact from charge annihilation, and this has been noted in multiple studies. The calcium binding site is also situated in the membrane water interface, where the dielectric constant is likely to be lower than expected in solvent. However, the relative binding free energy of calcium caused by the binding of PAM_16A is 10-14 kJ/mol on both the first and the second binding sites of calcium. This is approximately a 50-300 fold difference in calcium affinity. Thus, the calculation proposes that the mechanism of the drug is to increase TMEM16A affinity to calcium.

One interesting insight from the experimental study is that once the calcium concentration is saturated (12.5 μM), PAM_16A has no effect on the maximal current at +70 mV. This suggested that PAM_16A has no direct influence on calcium-dependent efficacy. The work also highlighted that at 300 nM PAM_16A or saturating concentration, the channel open probability could be increased up to 0.3. Multiple simulation methods have been used to predict the ligand's affinity, primarily on the D2 dopamine receptor using a series of swarms simulations, and on the β2-adrenergic receptor using an accelerated weighted histogram. However, direct use of simulation methods to predict the open probability of an

ion channel has not been demonstrated. In this study, FAST adaptive sampling has been used to evaluate the drug's effect on the channel's open probability. The free energy highlighted that when the channel is bound to calcium, the distribution between the open and closed states remains relatively similar in the presence and absence of PAM_16A. PIP_2 is not included in this study as the experimental data suggested that PIP_2 has no effect on the action of PAM_16A. In the absence of the ligand, FAST adaptive sampling fails to sample the opening of the outer gate and the kink at the TM6, whereas in the simulation with PAM_16A, the kink is being sampled and thus allows the steric gate to open. This is consistent with the increase in open probability occurring only in the absence of calcium. Overall, this explains the two modes of TMEM16A activation by PAM_16A: increasing the channel's open probability by acting on the steric gate in the absence of calcium and increasing TMEM16A's affinity for calcium.

The bottleneck in the activator design is that binding affinity does not always correlate with efficacy or potency. Most high-throughput drug discovery methods focus on affinity, but there is no easy way to calculate efficacy. The closest is to design a thermodynamic cycle and calculate the difference in binding free energy between the open and closed conformations. This work highlights that using FAST adaptive sampling in conjunction with FEP, I can disentangle affinity from efficacy and improve drug design. The pharmacological effect of a drug molecule can be inferred from electrophysiological evidence and thus can be used to cross-validate our identification of the drug binding site. The drug binding site can indeed be further verified using site-directed mutagenesis. This study provides a comprehensive framework for identifying the drug binding site and validating it using experimental parameters, rather than the traditional mutagenesis approach, which is only accessible experimentally. Together, this study shows that MD simulation with adaptive sampling and FEP can be used to dissect the mechanism of action of PAM_16A activator on TMEM16A, and open the opportunity to a new drug testing pipeline, independent of the traditional mutagenesis verification, yet still able to retrieve similar electrophysiological and pharmacological parameters.

Methods

System preparation and molecular dynamics simulation

The mouse TMEM16A with Ca^{2+} bound with 1PBC (PDB entry: 7zk3), with the drug molecule being removed [17] using Swissmodel [20] from residues 117-130 and 165-910. The protein was then embedded in POPC, TIP3P water, and 0.15 M NaCl using CHARMM-GUI Membrane Builder under the CHARMM36m force field. The system was then energy-minimised and equilibrated using the standard six steps CHARMM-GUI equilibration protocol [21]. This includes the following set-up: protein backbone was restrained at the force constant of 4000, 2000, 1000, 500, 200 and 50 $kJmol^{-1}\,nm^{-2}$, protein side chains were restrained at the force constant of 2000, 1000, 500, 200, 50, and 0 $kJmol^{-1}\,nm^{-2}$, non-H atoms of lipids were restrained at the force constant of 1000, 400, 400, 200, 40 and 0 $kJmol^{-1}\,nm^{-2}$, and dihedral restraints were set at the force constant of 1000, 400, 200, 200, 100 and 0 $kJmol^{-1}\,rad^{-2}$. Simulations were equilibrated with a 1 fs timestep for 125 ps for the first three steps, and then to a 2 fs timestep for 500 ps, the next two, and 10 ns for the final step. The first two steps were performed with the NVT ensemble, and the last four with the NPT ensemble. All equilibration runs were conducted at 310 K using a Berendsen thermostat [22]. In all NPT ensemble equilibration, the pressure was maintained at 1 bar using a Berendsen barostat [22]. All simulations were conducted using GROMACS-2023.4 [23]. All images from simulations were generated using PyMOL.

Chai-1 modelling

The sequence of the mouse TMEM16A was taken based on the PDB structure and was input to the webserver (https://lab.chaidiscovery.com/) to generate the PDB model. 20 ligands were added as part of the input for the binding site to be identified and the top 3 poses were then chosen for clustering analyses.

Coarse-grained MD simulation

TMEM16A were converted to the MARTINI3 coarse-grained force field using *martinize2.py* [24] with the elastic network cutoff at 0.8 nm. The protein was then embedded

in a palmitoyl-oleyl phosphatidylcholine (POPC) bilayer, or in a system with 100% POPC and coarse-grained water using *insane.py.* The coarse-grained PAM_16A parameter was generated using Automartini3. In the simulation box, 20 PAM_16A were placed randomly by replacing coarse-grained water particles using *gmx insert-molecule*. The system was energy-minimised using the steepest-descent algorithm and equilibrated for 50 ns [25]. The system was equilibrated at 323 K with v-rescale temperature coupling [26], and the pressure was maintained at 1.0 bar using Parrinello-Rahman pressure coupling [27]. To identify the PAM_16A binding site, the simulations were conducted for 10 μs. The binding site was obtained using PyLIPID, and the site with the highest occupancy and residence time was chosen [28].

Free energy perturbation of the calcium ion

The mouse TMEM16A with one or two Ca^{2+} ions bound with and without PAM_16A, obtained after equilibration, was used as the initial coordinates for FEP calculations. Here, I calculated the absolute binding free energy (ΔG) by converting from Ca^{2+} to a dummy atom along a reaction coordinate in a chemical space denoted λ. As is standard for FEP calculations, separate transformations were performed with calcium bound to the channel in 0.15 NaCl or in TIP3P water with no ions. The solvent bulk system is 3 x 3 x 3 nm^3 During the transformation, coulombic (charge interactions) and Lennard–Jones (van der Waals interactions) were turned off separately, with a soft-core parameter used for the Lennard–Jones interactions. The coulombic interactions were perturbed linearly (λ = 0, 0.025, 0.05 … 0.975, 1.0) in the first thirty simulation windows, with the van der Waals interactions perturbed linearly (λ = 0, 0.1, 0.2 …… 0.9, 1.0) in the last ten simulation windows with the soft-core parameters of α = 0.5 and σ = 0.3. A flat-bottom restraint was applied between E734 and Ca^{2+} with a 5 Å radius. Each simulation window was energy-minimised and equilibrated as described above, before three production runs of 15 ns were carried out with randomised initial velocities, using a leap-frog molecular dynamics integrator. This prevents bound Ca^{2+} from drifting away from its binding pocket, thereby increasing the accuracy of the calculation. The free energy pathways were constructed using the alchemical-analysis software package via gmx bar. The finite size effect were corrected using Rocklin correction. Each simulation was conducted in 3 replicates. Analyses were run using the MBAR. All values are reported as mean ± SD.

Adaptive sampling and MSM building

The FAST algorithm was used to adaptively sample the open state of the TMEM16A channel [29]. The distance between the carbon atoms on the C_α and the side chain of the residues lining (1) TM3 (Q637, I641, G644, K645 and Q649), TM4,6 (V543, L547, V548, V549, I551, D554, E555, A600, K603,); (2) TM4 (V543, L547, V548, V549, I551, D554, E555) and TM6 (V599, A600, K603); and (3) E555-L652 and E555-E654 was maximised over 15 iterations and minimised over 10 iterations. Each iteration was run for 50 ns, with a frame step of 0.5 ns. The Markov-state model (MSM) was built for each iteration, yielding no more than 500 clusters. Upon building the Markov State model, the free energy landscape was clustered into three distinct macrostates after 30 simulation cycles (10 towards closing and 20 towards opening). In the simulations where calcium is absent, only those favouring channel opening were conducted for 20 cycles. The complete set of pore-lining residue minimum distances (closest-heavy-atom scheme) was used to featurise each trajectory. The features were projected onto a lower-dimensional space using time-lagged independent component analysis (tICA) with a lag of 10 ns, retaining the 10 slowest independent components. The tICA space was discretised into 200 microstates by k-means clustering, and a maximum-likelihood MSM was estimated at a lag time of 10 ns (frame interval 0.5 ns). A Bayesian MSM was estimated with the same parameters to obtain statistical uncertainties. The MSM stationary distribution was used to reweight the sampled conformations, and the three metastable macrostates were extracted by PCCA++ coarse-graining. The MSM lag time was then validated using the implied-timescale (ITS) test: the slowest implied timescales became approximately independent of the lag time from ~10 ns onward, justifying the 10 ns production lag (Figures S4–S7). Markovianity of the three-macrostate model was confirmed with the Chapman–Kolmogorov (CK) test, in which MSM predictions agreed with direct estimates from the trajectories within the Bayesian confidence intervals. Outer-gate opening was quantified by the minimum distance between V543 and I640, and the steric-gate kink of TM6 by the Cα angle defined across residues 648, 656 and 664 (hinge at G656). Mean first-passage times between the three macrostates were computed from the MSM transition matrix. All MSM estimation, validation and analysis were performed with PyEMMA 2.5.7 [30], and trajectory featurisation with MDTraj.

421

422

References

1 Pedemonte, N. & Galietta, L. J. Structure and function of TMEM16 proteins (anoctamins). *Physiol Rev* **94**, 419-459 (2014). https://doi.org:10.1152/physrev.00039.2011

2 Duran, C. & Hartzell, H. C. Physiological roles and diseases of Tmem16/Anoctamin proteins: are they all chloride channels? *Acta Pharmacol Sin* **32**, 685-692 (2011). https://doi.org:10.1038/aps.2011.48

3 Caputo, A. *et al.* TMEM16A, A Membrane Protein Associated with Calcium-Dependent Chloride Channel Activity. *Science* **322**, 590-594 (2008). https://doi.org:10.1126/science.1163518

4 Yang, Y. D. *et al.* TMEM16A confers receptor-activated calcium-dependent chloride conductance. *Nature* **455**, 1210-1215 (2008). https://doi.org:10.1038/nature07313

5 Schroeder, B. C., Cheng, T., Jan, Y. N. & Jan, L. Y. Expression cloning of TMEM16A as a calcium-activated chloride channel subunit. *Cell* **134**, 1019-1029 (2008). https://doi.org:10.1016/j.cell.2008.09.003

6 Ta, C. M., Acheson, K. E., Rorsman, N. J. G., Jongkind, R. C. & Tammaro, P. Contrasting effects of phosphatidylinositol 4,5-bisphosphate on cloned TMEM16A and TMEM16B channels. *Br J Pharmacol* **174**, 2984-2999 (2017). https://doi.org:10.1111/bph.13913

7 Tembo, M., Wozniak, K. L., Bainbridge, R. E. & Carlson, A. E. Phosphatidylinositol 4,5-bisphosphate (PIP2) and Ca2+ are both required to open the Cl− channel TMEM16A. *Journal of Biological Chemistry* **294**, 12556-12564 (2019). https://doi.org:https://doi.org/10.1074/jbc.RA118.007128

8 Le, S. C., Jia, Z., Chen, J. & Yang, H. Molecular basis of PIP(2)-dependent regulation of the Ca(2+)-activated chloride channel TMEM16A. *Nat Commun* **10**, 3769 (2019). https://doi.org:10.1038/s41467-019-11784-8

9 Yu, K., Jiang, T., Cui, Y., Tajkhorshid, E. & Hartzell, H. C. A network of phosphatidylinositol 4,5-bisphosphate binding sites regulates gating of the Ca2+-activated Cl− channel ANO1 (TMEM16A). *Proceedings of the National Academy of Sciences* **116**, 19952-19962 (2019). https://doi.org:10.1073/pnas.1904012116

10 Peters, C. J. *et al.* The Sixth Transmembrane Segment Is a Major Gating Component of the TMEM16A Calcium-Activated Chloride Channel. *Neuron* **97**, 1063-1077.e1064 (2018). https://doi.org:10.1016/j.neuron.2018.01.048

11 Tien, J. *et al.* A comprehensive search for calcium binding sites critical for TMEM16A calcium-activated chloride channel activity. *eLife* **3**, e02772 (2014). https://doi.org:10.7554/eLife.02772

12 Lam, A. K. & Dutzler, R. Calcium-dependent electrostatic control of anion access to the pore of the calcium-activated chloride channel TMEM16A. *Elife* **7** (2018). https://doi.org:10.7554/eLife.39122

13 Dinsdale, R. L. *et al.* An outer-pore gate modulates the pharmacology of the TMEM16A channel. *Proc Natl Acad Sci U S A* **118** (2021). https://doi.org:10.1073/pnas.2023572118

14 Paulino, C., Kalienkova, V., Lam, A. K. M., Neldner, Y. & Dutzler, R. Activation mechanism of the calcium-activated chloride channel TMEM16A revealed by cryo-EM. *Nature* **552**, 421-425 (2017). https://doi.org:10.1038/nature24652

15 Dang, S. *et al.* Cryo-EM structures of the TMEM16A calcium-activated chloride channel. *Nature* **552**, 426-429 (2017). https://doi.org:10.1038/nature25024
16 Lam, A. K. M., Rheinberger, J., Paulino, C. & Dutzler, R. Gating the pore of the calcium-activated chloride channel TMEM16A. *Nature Communications* **12**, 785 (2021). https://doi.org:10.1038/s41467-020-20787-9
17 Lam, A. K. M., Rutz, S. & Dutzler, R. Inhibition mechanism of the chloride channel TMEM16A by the pore blocker 1PBC. *Nat Commun* **13**, 2798 (2022). https://doi.org:10.1038/s41467-022-30479-1
18 Feng, S. *et al.* Identification of a drug binding pocket in TMEM16F calcium-activated ion channel and lipid scramblase. *Nature Communications* **14**, 4874 (2023). https://doi.org:10.1038/s41467-023-40410-x
19 Al-Hosni, R. *et al.* Pharmacological profiling of small molecule modulators of the TMEM16A channel and their implications for the control of artery and capillary function. *Br J Pharmacol* **182**, 1719-1740 (2025). https://doi.org:10.1111/bph.17383
20 Waterhouse, A. *et al.* SWISS-MODEL: homology modelling of protein structures and complexes. *Nucleic Acids Research* **46**, W296-W303 (2018). https://doi.org:10.1093/nar/gky427
21 Wu, E. L. *et al.* CHARMM-GUI Membrane Builder toward realistic biological membrane simulations. *J Comput Chem* **35**, 1997-2004 (2014). https://doi.org:10.1002/jcc.23702
22 Berendsen, H. J. C., Postma, J. P. M., van Gunsteren, W. F., DiNola, A. & Haak, J. R. Molecular dynamics with coupling to an external bath. *The Journal of Chemical Physics* **81**, 3684-3690 (1984). https://doi.org:10.1063/1.448118
23 Abraham, M. J. *et al.* GROMACS: High performance molecular simulations through multi-level parallelism from laptops to supercomputers. *SoftwareX* **1-2**, 19-25 (2015). https://doi.org:https://doi.org/10.1016/j.softx.2015.06.001
24 Monticelli, L. *et al.* The MARTINI Coarse-Grained Force Field: Extension to Proteins. *Journal of Chemical Theory and Computation* **4**, 819-834 (2008). https://doi.org:10.1021/ct700324x
25 Wassenaar, T. A., Ingólfsson, H. I., Böckmann, R. A., Tieleman, D. P. & Marrink, S. J. Computational Lipidomics with insane: A Versatile Tool for Generating Custom Membranes for Molecular Simulations. *Journal of Chemical Theory and Computation* **11**, 2144-2155 (2015). https://doi.org:10.1021/acs.jctc.5b00209
26 Bussi, G., Donadio, D. & Parrinello, M. Canonical sampling through velocity rescaling. *J Chem Phys* **126**, 014101 (2007). https://doi.org:10.1063/1.2408420
27 Parrinello, M. & Rahman, A. Polymorphic transitions in single crystals: A new molecular dynamics method. *Journal of Applied Physics* **52**, 7182-7190 (1981). https://doi.org:10.1063/1.328693
28 Song, W. *et al.* PyLipID: A Python Package for Analysis of Protein–Lipid Interactions from Molecular Dynamics Simulations. *Journal of Chemical Theory and Computation* **18**, 1188-1201 (2022). https://doi.org:10.1021/acs.jctc.1c00708
29 Zimmerman, M. I. & Bowman, G. R. FAST Conformational Searches by Balancing Exploration/Exploitation Trade-Offs. *Journal of Chemical Theory and Computation* **11**, 5747-5757 (2015). https://doi.org:10.1021/acs.jctc.5b00737
30 Scherer, M. K. *et al.* PyEMMA 2: A Software Package for Estimation, Validation, and Analysis of Markov Models. *Journal of Chemical Theory and Computation* **11**, 5525-5542 (2015). https://doi.org:10.1021/acs.jctc.5b00743

513

514

515

516

Figures and Tables

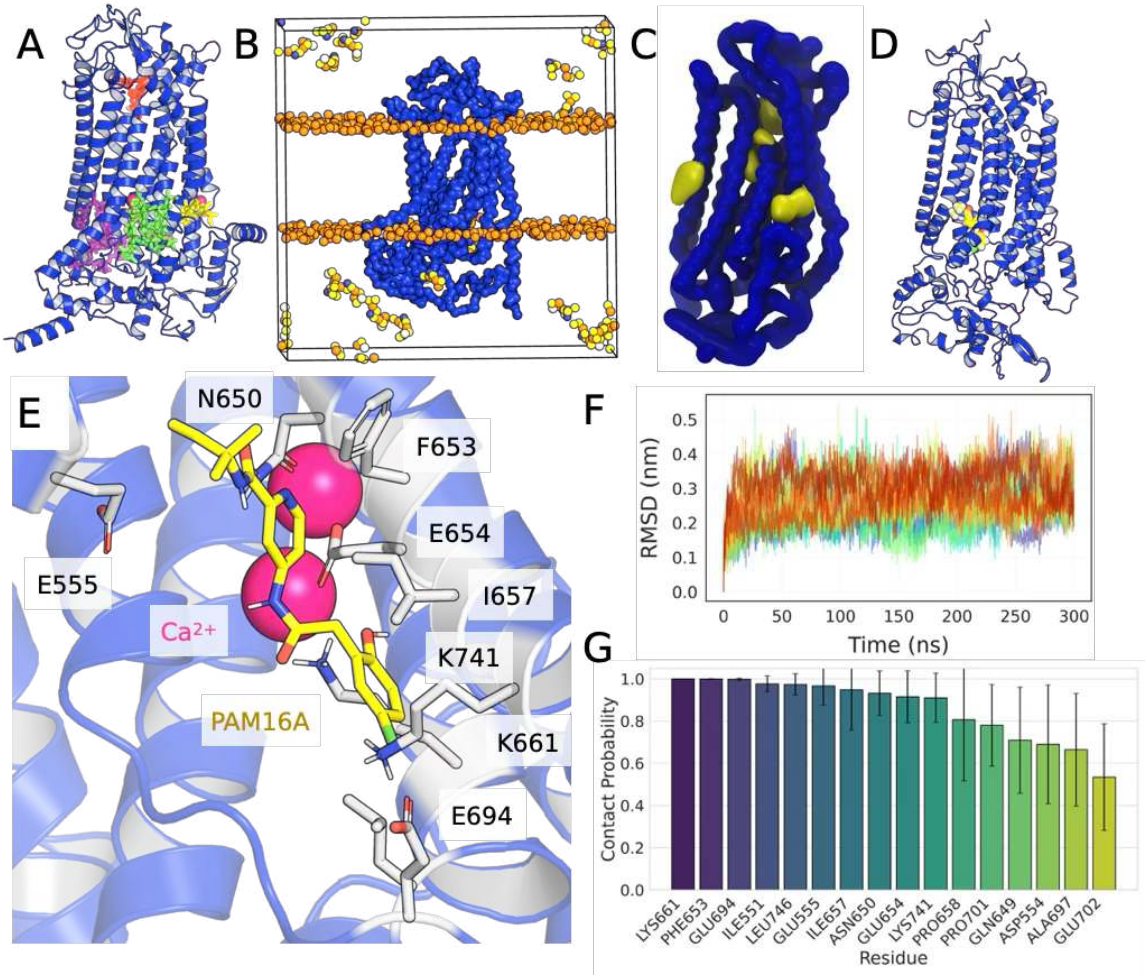


Figure 1. Identification of the PAM_16A binding site near the calcium-binding site of TMEM16A. (A) Chai-1 predicted poses for PAM_16A on a TMEM16A monomer, clustering at two intracellular regions: the steric gate (between TM4 and TM6) and in front of the calcium-binding site on TM6. (B) MARTINI-3 coarse-grained flooding simulation, with 20 PAM_16A molecules randomly placed in the simulation box around the channel (10 replicates of 10 μs). (C) Coarse-grained PAM_16A density (VolMap), clustered at the calcium-binding site and the steric gate. (D) Top-ranked docking pose of PAM_16A at the calcium-binding site. (E) Representative all-atom binding pose: PAM_16A (yellow) occupies a pocket adjacent to the two calcium ions (magenta), formed by hydrophobic residues (I551, F653, I657, L746), with the chlorine atom near K661 and hydrogen bonds to K671/K741, N650, E555 and E654. (F) RMSD of PAM_16A relative to the docking pose across 15 independent 300 ns simulations; most values remain below 0.4 nm. (G) Per-residue contact probability between PAM_16A and the channel, averaged over the 15 replicates.

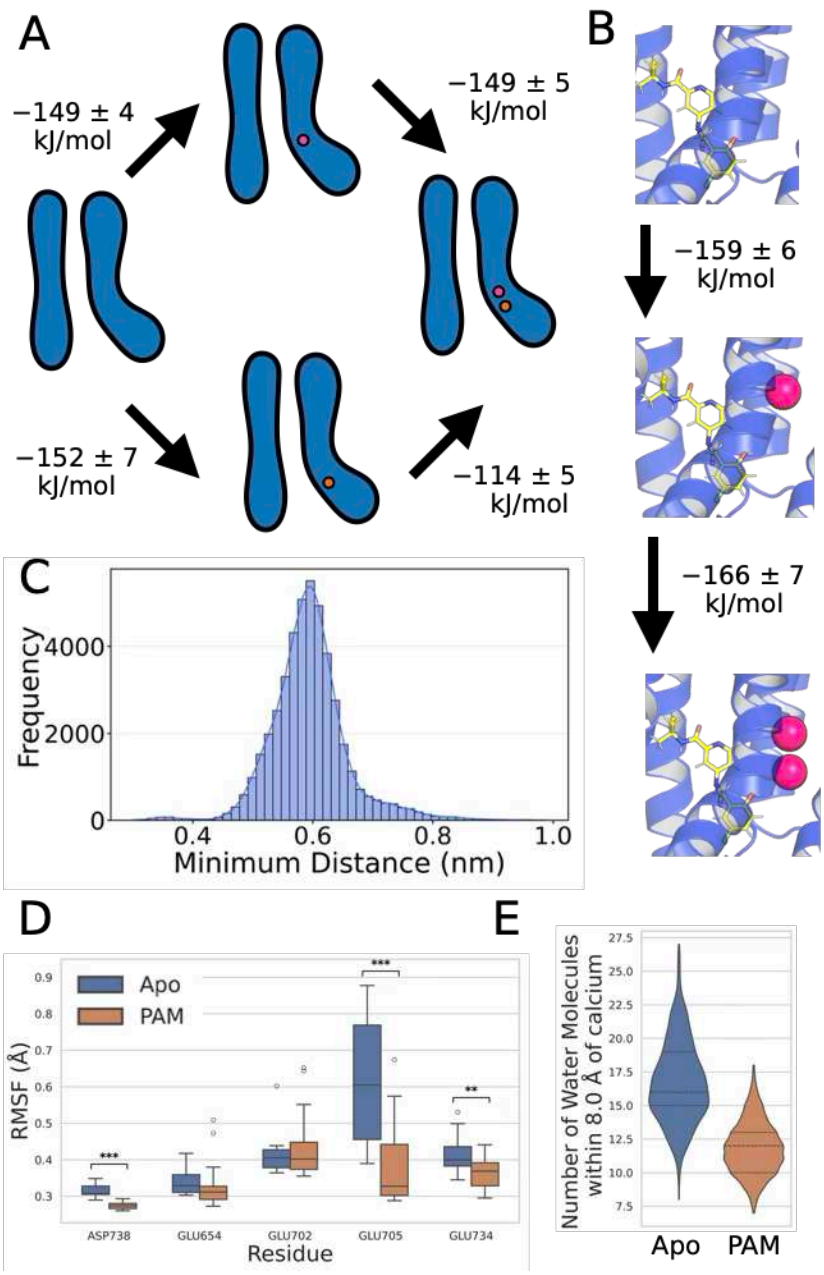


Figure 2. PAM_16A increases the calcium affinity of TMEM16A. (A) Absolute calcium binding free energies (ΔG) from free energy perturbation (FEP) for the channel without drug, showing the calcium binding order: with a single ion bound the top and bottom sites have comparable affinity (−149 ± 4 and −152 ± 7 kJ/mol), whereas occupation of the partner site weakens the top site (−114 ± 5 kJ/mol), indicating the top site is filled first. (B) Calcium binding free energies in the presence of PAM_16A (yellow; calcium in magenta); affinity increases by ~10–14 kJ/mol per ion (−159 ± 6 and −166 ± 7 kJ/mol). (C) Distribution of the minimum distance between PAM_16A and the bound calcium ion over 15 × 300 ns simulations (peak ≈ 0.6 nm). (D) Side-chain RMSF of calcium-coordinating residues

without (Apo) and with (PAM) drug; fluctuations are significantly reduced, notably at E705, E734 and D738. (E) Number of water molecules within 8 Å of the bound calcium for Apo versus PAM, showing dehydration of the pocket upon PAM_16A binding (≈16 versus ≈12). FEP values are mean ± SD of n = 3 independent replicates; **p < 0.01, ***p < 0.001.

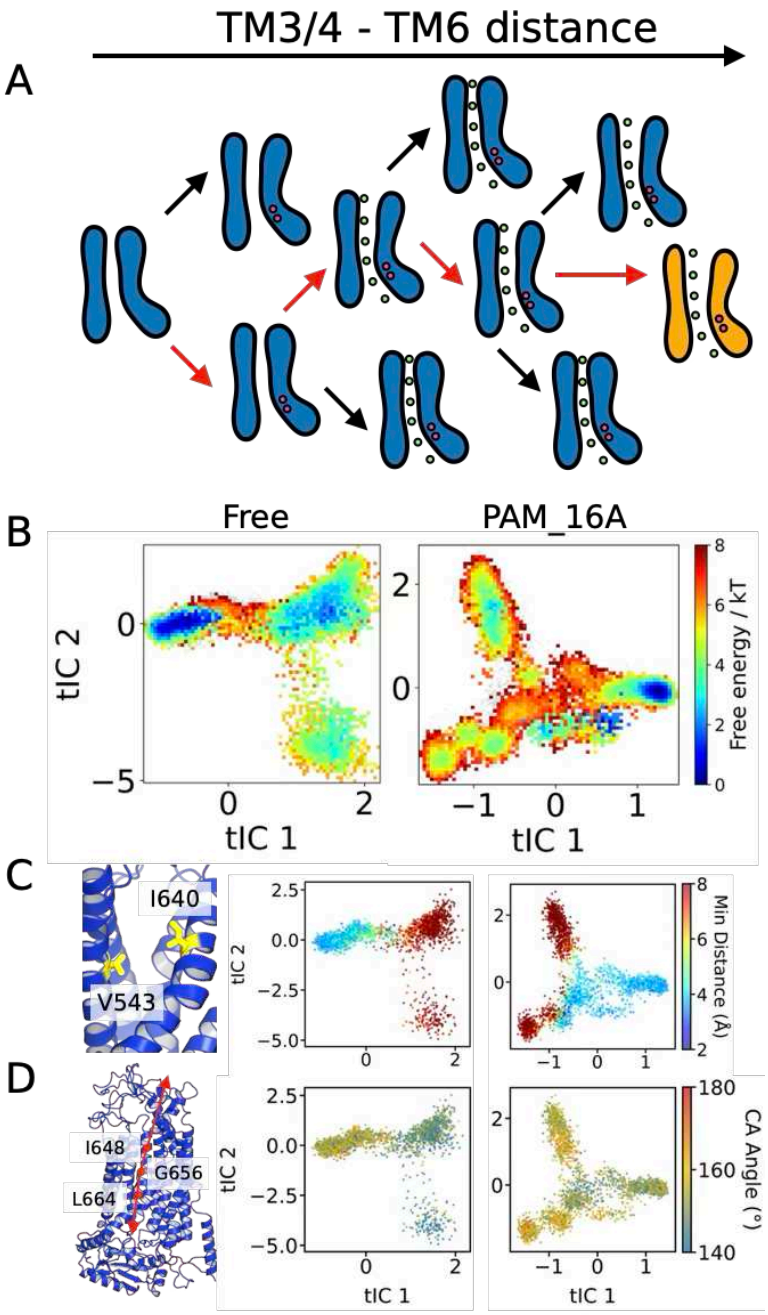


Figure 3. PAM_16A does not alter the open-state distribution of calcium-bound TMEM16A. (A) Schematic of the outer-gate opening pathway driven by FAST adaptive sampling, parameterised along the TM3/4–TM6 distance. (B) Free energy landscape projected onto the first two time-lagged independent components (tICA) for the calcium-bound channel in the absence (Free) and presence (PAM_16A) of the drug; three minima of comparable depth are resolved in both conditions. (C) The same landscape coloured by the minimum distance between V543 and I640 (outer-gate metric) and (D) by the TM6 Cα kink angle around G656 (steric gate metric).

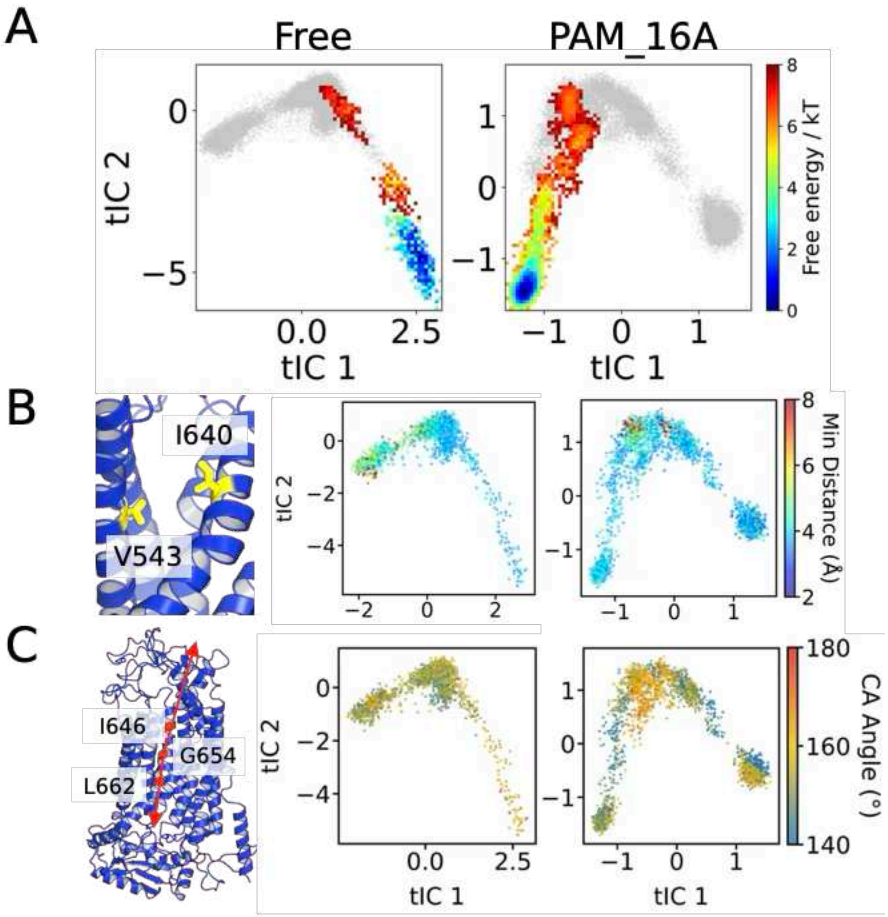


Figure 4. PAM_16A stabilises the TM6 kink without dilating the outer gate in the absence of calcium. (A) Free energy landscape (tICA) for the calcium-free channel without (Free) and with (PAM_16A) the drug. (B) The landscape coloured by the V543–I640 outer-gate distance and (C) by the TM6 Cα kink angle. In the presence of PAM_16A, a ~160-170° kink of TM6 (steric gate) is sampled while the outer gate remains undilated, consistent with the modest, calcium-independent increase in open probability observed experimentally.

Supplementary Files

This is a list of supplementary files associated with this preprint. Click to download.

- SIPAM16A050726.pdf
- SIPAM16A050726.pdf